

Fine-tuning of the electro-optical switching behavior in indium tin oxideIvan A. Pshenichnyuk ^{1,*}, Sergey S. Kosolobov ¹ and Vladimir P. Drachev ^{1,2}¹*Skolkovo Institute of Science and Technology, Moscow 121205, Russian Federation*²*University of North Texas, Denton, Texas 76203, USA*

(Received 19 August 2020; revised 9 December 2020; accepted 3 February 2021; published 4 March 2021)

Indium tin oxide is often used as an active material in photonics. Strong correlation between its optical response and a state of conduction electrons, as well as an intermediate density of charges typical for semiconductors, makes it highly tunable using an external electric field. This property is extensively used in various types of electro-optical modulators. Usually for infrared switching the charge concentration is manipulated in order to reach the epsilon-near-zero regime, where the real part of permittivity is small and losses are high. This allows one to switch between an optically transparent state and a highly absorbing state. In this paper we investigate the possibility of a different switching mechanism, namely, between the state where the propagation of surface plasmons is possible and another state where surface waves are forbidden. To obtain modes with high quality factors, which is challenging in indium tin oxide, we suggest using odd pairs of surface plasmons supported by thin films. The accumulation layer, formed at the boundary between indium tin oxide and the insulator under the influence of an external voltage, is considered as a tunable plasmonic waveguide. Both analytical and numerical analysis is used, first, to localize the regime where such modes are possible and, second, to compute the characteristics of corresponding plasmons in realistic conditions. Drift-diffusion equations and Maxwell equations are solved numerically in a self-consistent way to handle electronic and optical aspects of the problem. High tunability of plasmonic modes is demonstrated in infrared. The obtained results can be implemented in the new generation of plasmonic modulators and electro-optical circuits.

DOI: [10.1103/PhysRevB.103.115404](https://doi.org/10.1103/PhysRevB.103.115404)**I. INTRODUCTION**

Modern photonics requires fast and compact electro-optical components for further development. Today, in most applications, their performance is limited by the laws of classical optics and electronics [1,2]. To overcome the restrictions, it is necessary to search for the regimes of efficient light-matter interaction at the edge of classical physics and beyond. One elegant approach available today suggests the exploitation of hybrid quasiparticles assembled from both electrons and photons [3–5]. One such hybrid under active investigation is an exciton-polariton (EP). It possess a number of peculiar properties such as, for example, the ability to form Bose-Einstein condensate at room temperature [6]. In the condensed state it demonstrates a coherent behavior typical for quantum fluids and supports a number of nonlinear excitations, such as solitons [7] and quantum vortices [8–10]. Some potential applications of exciton-polaritons have already been suggested [11,12]. Another peculiar quasiparticle is a plasmon polariton. Hybridization of light with oscillations of electron plasma and resulting hybrid modes, such as surface plasmon polaritons (SPPs), demonstrate a number of useful properties [13]. Compactness below the diffraction limit and the strong light-matter interaction achievable in these modes allow plasmonic devices to be made smaller and faster [14–16].

The useful property of strongly hybridized states is the ability to influence one component of the mixture, manipulating the other. This principle is quite promising for future electro-optical devices and, in particular, modulators [17]. Plasmonic frequency, which defines the optical response of a large class of materials in infrared, depends on the density of charge carriers. Tuning the density via standard mechanisms used in electronics, such as, for example, applying the voltage, one may change the optical response. This mechanism is extensively used in various plasmonic devices to perform switching [18–23].

The choice of an active material in such devices is not a trivial problem. Classical plasmonic materials are mainly metals, such as, for example, gold and silver. They support SPP modes of high quality. At the same time, the concentration of charges is high there, and one cannot change much the relative distribution of charges applying voltages that are reasonable in electronics (tens of volts). For this reason, metals are in general bad switchers. Insulators cannot be used either. If the density of electrons is too small, plasmonic properties of the material become negligible. Materials with good plasmonic switching behavior should be searched for among semiconductors, with intermediate and well-controlled charge density. The concentration profiles and corresponding optical properties can vary significantly there under the influence of external fields.

One popular active material that was successfully used in various models of modulators is indium tin oxide (ITO) [24–26]. It is highly tunable. An external voltage can be

*Corresponding author: i.pshenichnyuk@skoltech.ru

used to cause two-orders-of-magnitude local charge density variation. It influences plasmonic frequency and permittivity a lot and can be used to construct active devices [27]. At the same time, ITO is not considered as a good SPP supporting material [28], and there are a few reasons for that. To obtain propagating plasmonic modes in the popular C + L telecom range, one should reach an extreme level of doping, close to the maximal possible in ITO. Even when this criterion is fulfilled, the quality factors, i.e., the propagation length relative to the size of the mode, are usually poor. On the other hand, to provide switching in ITO, the epsilon-near-zero (ENZ) effect is often utilized [29,30]. The combination of a large imaginary part and a small real part of permittivity causes significant variation in the optical response in this regime. The charge density required to switch on ENZ is always smaller in ITO than the concentration required to make SPP modes possible.

Practically, only a small fraction of bulk ITO is tunable using an external voltage. A thin insulating layer incorporated into a semiconductor is usually used as a capacitor to collect the necessary charge density [21]. The detailed calculations show that the width of the layer with modified properties in this case is of the order of nanometers. Nevertheless, it is enough to switch between the almost transparent state and the highly absorbing state of ENZ modulators [23]. At the same time, the existence of a very thin and highly tunable accumulation layer in ITO suggests the alternative idea of using it as an SPP supporting structure. SPP modes in very thin films are successfully studied in such materials as graphene [31,32]. Much thicker film plasmons are also studied experimentally in ITO [33,34]. Tunable plasmons in nanorods made from ITO are investigated [35]. However, to the best of our knowledge, there is no comprehensive theoretical study investigating the possibility to use the accumulation layer as a tunable plasmonic waveguide. In the case of ITO, thin film plasmons have a different dispersion relation compared with single-interface surface waves and possess a much better quality. High tunability of the layer allows one to switch the existence of the SPP supporting channel, instead of switching the absorption. The appropriate usage of these modes in plasmonic waveguides would make them *a priori* tunable, without the necessity to use special devices for electro-optical modulation. Electrical contacts attached to such a waveguide can be used to manipulate the signal. In this paper we investigate the possibility to realize the described switching mechanism.

Our paper has the following structure. In Sec. II we overview the plasmonic properties of ITO and describe its permittivity for different levels of doping. Characteristics of surface waves and their quality factors in different regimes are analyzed. In Sec. III we analyze numerically and analytically dispersion curves for SPP modes in thin films and demonstrate their advantages for applications compared with single-interface waves. The theory is applicable to two different cases. It describes SPP modes in thin films of highly doped ITO surrounded by a dielectric (untunable case). It also approximately describes plasmons supported by the accumulation layers created in ITO with low doping level at a boundary with a dielectric using voltage (tunable case). In Sec. IV we discuss the properties of a hybrid plasmonic waveguide with an embedded thin film mode. Such a waveguide represents one simple example of a device available for

experimental realization and verification of the presented theoretical results. The conversion between classical waveguide modes and thin film plasmons is discussed. Qualitative difference between SPP and ENZ regimes in ITO is demonstrated. In Sec. V we discuss the tunability of thin film SPP modes numerically using a realistic model based on drift diffusion and Maxwell equations. The obtained results are compared with the simplified theory presented in Sec. III. Charge density profiles for accumulation layers formed at ITO-insulator boundaries are obtained for different voltages and geometries. The possibility to manipulate plasmons using the voltage is demonstrated.

II. SPP MODES IN ITO

The concentration of electrons in ITO can be varied by applying external electric fields (locally) or using doping. The experimentally available range of concentrations in the latter case varies between 10^{18} and $3 \times 10^{21} \text{ cm}^{-3}$ [36]. In this section we provide an overview of the plasmonic properties of ITO in a whole range of relevant concentrations.

The permittivity of ITO in the infrared range is well approximated using the Drude formula [37]

$$\varepsilon(\omega) = \varepsilon_\infty - \frac{\omega_p^2}{\omega^2 + i\omega\gamma} \quad (1)$$

with three parameters: plasmonic frequency $\omega_p = \sqrt{n_c e^2 / (\varepsilon_0 m^*)}$, Drude damping constant $\gamma = e / (\mu_n m^*)$, and asymptotic permittivity $\varepsilon_\infty = 3.9$. Thus, to describe an optical response of ITO, it is necessary to define a concentration of electrons n_c , mobility μ_n , and effective mass m^* . It is known that the last two parameters vary slightly with the level of doping [36]. Taking into account experimental parameters, we plot the permittivity of ITO for different levels of doping in Fig. 1(a). Relevant ranges of frequencies such as near infrared (NIR, 0.7-3 μm), midinfrared (MIR, 3-8 μm), and C + L are shown by shaded areas.

The brown line represents the maximal achievable doping in ITO. One may obtain slightly higher electron concentrations in a thin layer at the boundary with a dielectric, applying a voltage. Nevertheless, this improvement is limited by values of voltage reasonable in modern electronics. For example, doubling the concentration and reaching $6 \times 10^{21} \text{ cm}^{-3}$, according to our computations, require a voltage around 15 V (assuming a 10-nm layer of high-quality HfO_2 dielectric and maximal initial doping level $3 \times 10^{21} \text{ cm}^{-3}$). This is close to the maximum of what we can practically expect.

In Fig. 1 we highlight the existence of two important points: ENZ frequency ω_{enz} and SPP upper boundary ω_{spp} . For the concentration 10^{21} cm^{-3} (blue line) they are shown using blue dots. The first point represents the frequency where the real part of the permittivity goes to zero.

$$\omega_{enz} = \sqrt{\frac{\omega_p^2}{\varepsilon_\infty} - \gamma^2}. \quad (2)$$

This point is characterized by the minimal refraction index $n = \text{Re}(\sqrt{\varepsilon})$ and high absorption, given by the imaginary part of the permittivity (not shown). These properties are good for switching. Using voltage to vary the concentration between

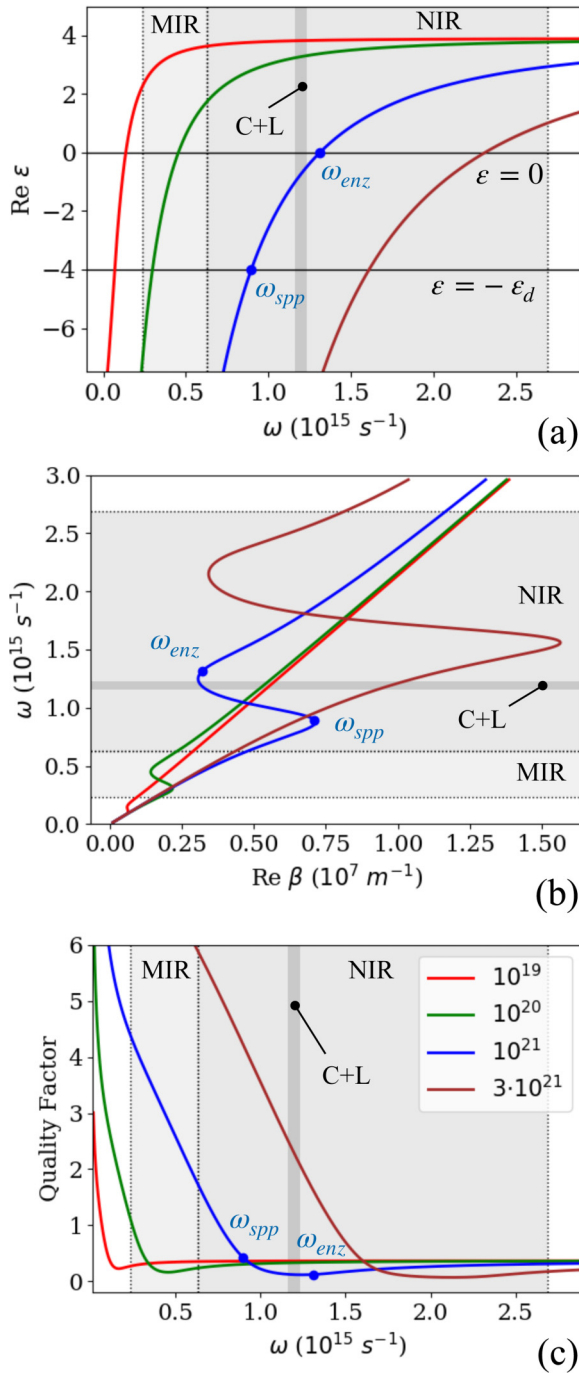


FIG. 1. Properties of SPP modes for ITO. (a) Permittivity of ITO with different doping levels. (b) Dispersion curves of SPP modes at the boundary between ITO and the dielectric. (c) Quality factors of single-interface plasmons in ITO.

the red line, which provides negligible absorption in the C + L range, and some value close to the blue line, one may switch on a thin but highly absorbing layer.

The meaning of the second point becomes clear when we consider the dispersion relation for SPP [1]

$$\beta = \frac{\omega}{c} \sqrt{\frac{\epsilon(\omega)\epsilon_d}{\epsilon(\omega) + \epsilon_d}}. \quad (3)$$

Parameter ϵ_d stands for the permittivity of the dielectric in contact with ITO, and β is the propagation constant of the surface wave. The dispersion curves are plotted for considered values of concentration in Fig. 1(b). One of the requirements for SPP modes to exist is the negative number in the denominator of Eq. (1), which is possible when $\epsilon < -\epsilon_d$ (see Ref. [1] for details). It is easy to show that surface modes exist below the frequency

$$\omega_{spp} = \sqrt{\frac{\omega_p^2}{\epsilon_\infty + \epsilon_d} - \gamma^2}. \quad (4)$$

The position of this point depends on the permittivity of the dielectric. In principle, it can be air, but in practical applications it is usually something more optically dense. For simplicity we consider $\epsilon_d = 4$.

The existence of both points is attributed to the same bulk plasmonic resonance, mathematically expressed by a complex Lorentzian [Eq. (1)] with position $\omega = 0$, amplitude ω_a , and width γ . The real part of the distribution in the physical half plane ($\omega > 0$) is plotted in Fig. 1(a). The position of the plasmonic peak is defined by free Drude electrons that do not have the eigenfrequency and can only feel the damping force proportional to γ . It is different, for example, for excitonic resonances with well-defined frequency and corresponding nonzero position. It is also different for SPP modes, since the position of such resonances is characterized by ω_{enz} or ω_{spp} [one may say that the resonance is located between these two points; see Fig. 1(b)] and depends on ω_p . For narrow resonances, when γ can be neglected, SPP resonance position is simply proportional to ω_p [see Eqs. (2) and (4)]. This means that both points move with the concentration n_e , but an optical behavior associated with them is very different. In particular, no SPP modes exist in the vicinity of ω_{enz} , but they are possible below ω_{spp} . The range between both points is usually considered as a forbidden optical band. The attenuation is maximal there. Modes above ω_{enz} are called Brewster modes and are not surface waves [1].

Figure 1(b) shows that for smaller concentrations such as 10^{19} and 10^{20} cm^{-3} (red and green lines, respectively), all plasmonic features in ITO belong to the MIR range and below. The concentration close to the maximal (brown line) is required to make SPP modes available in the C + L range. At the same time, ENZ concentration is slightly below 10^{21} cm^{-3} (blue line). This fact makes the ENZ regime more easily reachable; however, technically, SPP modes are possible, and varying the concentration between the maximal value and some smaller-value one can switch SPP modes on and off.

The surface plasmon propagation constant [Eq. (3)] can be used to define the propagation length L , size S , and quality factor Q in the following way [1,38]:

$$L(\omega) = [\text{Im}\beta(\omega)]^{-1}, \quad (5)$$

$$S(\omega) = \frac{1}{\text{Im}\sqrt{\frac{\omega^2}{c^2}\epsilon_d - \beta^2(\omega)}} + \frac{1}{\text{Im}\sqrt{\frac{\omega^2}{c^2}\epsilon(\omega) - \beta^2(\omega)}}, \quad (6)$$

$$Q(\omega) = L(\omega)/2S(\omega). \quad (7)$$

The quantity Q is plotted for different concentrations in Fig. 1(c). Even when the concentration is high, propagation

length does not exceed several times its own size. It is hard to reach quality factors larger than 3 in $C + L$ for these modes. For this reason, ITO is usually not considered to be a good SPP supporting material but rather is considered to be an ENZ material [28].

Another challenge which appears when one wants to create tunable SPP modes in ITO is the thickness of the accumulation layer under control, which is quite small. To switch on the absorption mechanism using ENZ, a layer that is a few nanometers thick but highly absorbing is enough [23]. On the other hand, the classical SPP mode [with dispersion given in Eq. (3)] requires one single ITO-dielectric interface. This suggests an idea to consider thin film surface waves instead. As we show in the next section, they are perfect candidates for tunable surface modes in ITO.

III. THIN FILM PLASMONS IN ITO

In this section we analyze plasmons in thin films of ITO. A large concentration of electrons $n_c = 3 \times 10^{21} \text{ cm}^{-3}$ and thicknesses in the range of 1-20 nm are considered. Such films can be practically realized in two ways. A thin film of highly doped ITO surrounded by relatively thick layers of dielectric with permittivity ϵ_d can be experimentally obtained using various deposition techniques [39–42]. Alternatively, undoped ITO can be used as a cladding material. As is shown in Fig. 1(a), a low concentration of electrons, such as 10^{19} cm^{-3} , guarantees almost dielectric constant permittivity in the NIR range. Its numerical value is close to the permittivity of popular dielectrics, such as SiO_2 and HfO_2 . The second way assumes the usage of an external field to create a thin accumulation layer with the required concentration. In this case a layer of high-quality dielectric should be incorporated between claddings made of undoped ITO. Such a structure works as a capacitor, allowing the necessary charge to accumulate at the ITO-dielectric boundary. To compare with the first case, it is a challenge to create accumulation layers thicker than a few nanometers. However, they are still thicker than, for example, sheets of graphene and are sufficient to support plasmonic modes (more in Sec. V). The second case is much more interesting, since the accumulation layer can be assembled and disassembled with a very high frequency. According to our evaluations, the layer formation time is of the order of picoseconds [23]. This mechanism can be utilized to control SPP modes. In this section we assume for simplicity that the concentration profile inside the layer is constant. The influence of charge distribution inside the layer on the properties of plasmons is discussed in the last section.

It is known that in structures with two interfaces, pairs of SPP modes hybridize to form even and odd combinations. When the distance between interfaces (i.e., the film thickness) becomes small, the dumping of even solutions increases, while the dumping of odd modes becomes small and allows them to propagate much farther. The dispersion relation for odd modes $\omega(\beta_f)$ is a solution of the algebraic equation [43]

$$\tanh\left(\frac{d}{2}\sqrt{\beta_f^2 - \frac{\omega^2}{c^2}\epsilon(\omega)}\right) + \frac{\epsilon_d\sqrt{\beta_f^2 - \frac{\omega^2}{c^2}\epsilon(\omega)}}{\epsilon(\omega)\sqrt{\beta_f^2 - \frac{\omega^2}{c^2}\epsilon_d}} = 0. \quad (8)$$

In our model, parameter d corresponds to the thickness of the film. The notation β_f is used for the propagation constant of thin film SPP (FSPP) modes.

For small d , one may decompose the hyperbolic tangent and solve the equation analytically. After certain simplifications the following dispersion relation can be derived:

$$k_x^2 = \frac{\omega^2}{c^2}\epsilon_d + \frac{\eta^4}{2\eta^2 + 4\xi^2}, \quad (9)$$

where

$$\eta \equiv \frac{\omega}{c}\sqrt{\epsilon(\omega) - \epsilon_d} \quad (10)$$

and

$$\xi \equiv \frac{1}{d}\frac{\epsilon(\omega)}{\epsilon_d}. \quad (11)$$

The resulting FSPP dispersion relation is plotted for a few different values of thickness in Fig. 2(a). An ordinary SPP mode is plotted for comparison using a brown line. Figure 2(a) shows that FSPP modes are essentially different compared with SPP. The group of thin film solutions is shifted towards higher frequencies. In general, this means that FSPPs require a lower electron concentration than SPPs to appear in the same frequency range.

It should be stressed that Eq. (9) becomes less reliable when the thickness of the layer becomes larger than 20 nm. A comparison between the analytical formula and numerical solution of Eq. (8) obtained using the secant method is shown. Starting from $d = 10$ nm and less, the precision of the analytical calculation becomes excellent. The validity of Eq. (9) is also confirmed by numerical simulations of FSPP modes in COMSOL MULTIPHYSICS. Effective mode indices obtained using both methods coincide.

It is clear from Eq. (9) that for $d = 0$ we obtain a plane-wave solution (first term). Moreover, decreasing d is accompanied by smooth transformation of the FSPP into a plane wave with corresponding delocalization of the mode. At the same time, even for $d = 1$ nm we still observe localized surface waves with a localization length of the order of micrometers. This last statement we prove by visualizing the quantity $\beta_f - \frac{\omega}{c}\sqrt{\epsilon_d}$ in Fig. 2(b). The green curve corresponding to $d = 1$ nm is easily distinguishable from the vertical line. Green and magenta dots show the solutions obtained using a fully numerical eigenmode solver. They coincide well with the analytical values.

FSPP modes as well as SPP modes have the upper limiting frequency which is shown using the horizontal red line in Fig. 2(b). Above this line the dumping coefficient (represented by the imaginary part of the propagation constant, not shown here) passes through zero and then becomes negative. Such modes are described in the literature [1,44]. They are not useful in the sense that they require a practically unrealizable excitation condition, and we do not consider them here. Two examples of the field distribution in FSPP modes are demonstrated in Figs. 2(c) and 2(d) for $d = 5$ nm. The corresponding positions of the plasmons are shown by arrows on the dispersion curve [Fig. 2(b)]. As in the case of ordinary SPP, modes with frequency approaching the upper limit (red line) are characterized by large dumping and small propagation length.

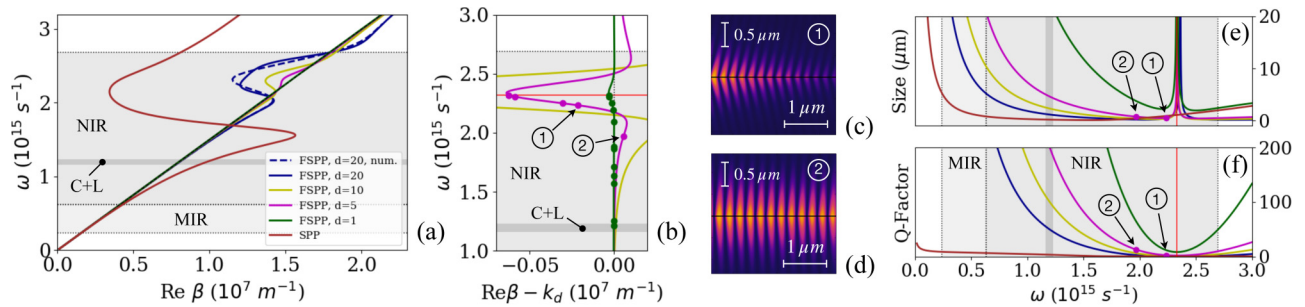


FIG. 2. Properties of thin film plasmons in ITO. (a) Dispersion curves of FSPP modes for different widths of the supporting layer. The single-interface SPP mode (brown line) is plotted for comparison. (b) Dispersion curves in a modified axis allow us to visualize, among other things, the curve for a 1-nm-wide layer (green line). (c) and (d) Field distributions for two specific FSPP modes denoted as “1” ($\lambda = 843 \text{ nm}$) and “2” ($\lambda = 957 \text{ nm}$) at the dispersion curve (magenta line, 5-nm-wide layer). (e) and (f) Size and quality factors of FSPP modes compared with a single-interface SPP mode (brown line).

The size and quality factors of FSPP modes [shown in Figs. 2(e) and 2(f)] can be evaluated using the propagation constant β_f as was described in the previous section. The FSPP is a hybridized pair of plasmons which exist inside the film and in both surrounding half planes. The SPP is a single mode, and its size is mainly concentrated in a dielectric half plane (the size of the part inside ITO is much smaller). To compare both modes, we calculate the size of the FSPP mode only in one half plane. Please note the factor of 2 in Fig. 2(e) for the whole FSPP mode. The plots demonstrate the fact that the quality factors for FSPP are much larger than for SPP. They also grow fast for large wavelengths and small layer thicknesses. Thus, decreasing the thickness, one may obtain very high values. Combining this principle with other methods to increase the propagation length may allow one to reach even more impressive results [45]. At the same time, the size of FSPP modes also grows for thinner layers. A size of the order of micrometers is quite affordable for waveguiding and signal transmission applications. We should note also that the quality factors grow much faster than size. So, in general, a reasonable balance may be achieved. Since the size of FSPP modes is significantly larger than the expected experimental inaccuracy in the fabrication of ITO-insulator interfaces (about 10 nm), such modes are particularly robust to various surface imperfections and roughness. The question of stability is additionally discussed in Appendix.

IV. IMPLEMENTATION OF FSPP IN HYBRID PLASMONIC WAVEGUIDES

In this section we demonstrate how a thin FSPP supporting layer with sufficient charge density can be practically used. The tunability of the layer and possible ways to manipulate it are discussed in the next section. For the demonstration we choose a 5-nm-thick layer with density $3 \times 10^{21} \text{ cm}^{-3}$ as described in the previous section. The FSPP mode with a wavelength $\lambda = 957 \text{ nm}$ is considered, corresponding to the example in Fig. 2(d). Its position at the dispersion curve is shown in Fig. 2(b). The mode is characterized by the propagation length $19 \mu\text{m}$, size $0.75 \mu\text{m}$, and corresponding quality factor 12.6. Thus the propagation length is not very large, but it is useful for visualization. The mode also has a convenient plasmon-waveguide conversion length (see below).

Alternatively, using the results of the previous section, any available FSPP with a desired quality factor can be selected. The qualitative results of the present section remain valid. To obtain the results of this section, we used eigenmode and frequency domain Maxwell solvers realized in COMSOL MULTIPHYSICS. A detailed mathematical description can be found in our previous work [23].

FSPP modes can be excited using appropriately designed grating couplers. Their quality factors are sufficient to make them attractive for applications such as, for example, on-chip communication. Nevertheless, at the present time it is hard to implement purely plasmonic optical circuits because of Ohmic losses. Large-scale circuits have to combine integrated photonics and plasmonics together [5]. The idea of finding a balance between the low losses of integrated silicon photonics and the high performance of plasmonics leads to the concept of hybrid plasmonic waveguides (HPWGs) [46,47]. For a practical realization of HPWG-based devices it is important to know how FSPP modes interact with more conventional waveguide modes and how they can be converted from one to the other.

In Fig. 3(a) we show what happens when we add a thin FSPP layer into a waveguide (the layer is shown with yellow). The waveguide is made of a material with permittivity ϵ_d and surrounded by air. Equations are solved in two dimensions (2D), assuming that the system is infinite and homogeneous in the direction perpendicular to the figure. The resulting HPWG contains at least two interacting p -polarized modes. When the waveguide mode feels the presence of the layer, modes hybridize. The subsequent propagation is accompanied by periodic conversions between what we call the “mainly waveguide” mode and the “mainly plasmonic” mode (during the propagation, the original modes are mixed and cannot be completely distinguished). The process is qualitatively similar to the propagation of waves in coupled waveguides. Unfortunately, the analytical theory of coupled waves is not appropriately generalized yet to describe plasmonic modes [46].

Field profiles of the pure FSPP mode and the waveguide mode are shown in Fig. 3(b). The fundamental p -polarized mode of the selected 1900-nm-wide waveguide has the effective index $n_{\text{eff}} = 1.9848$. This is close to the effective index of the FSPP, $n_{\text{eff}} = 2.0088 - 0.008i$, which allows the modes to

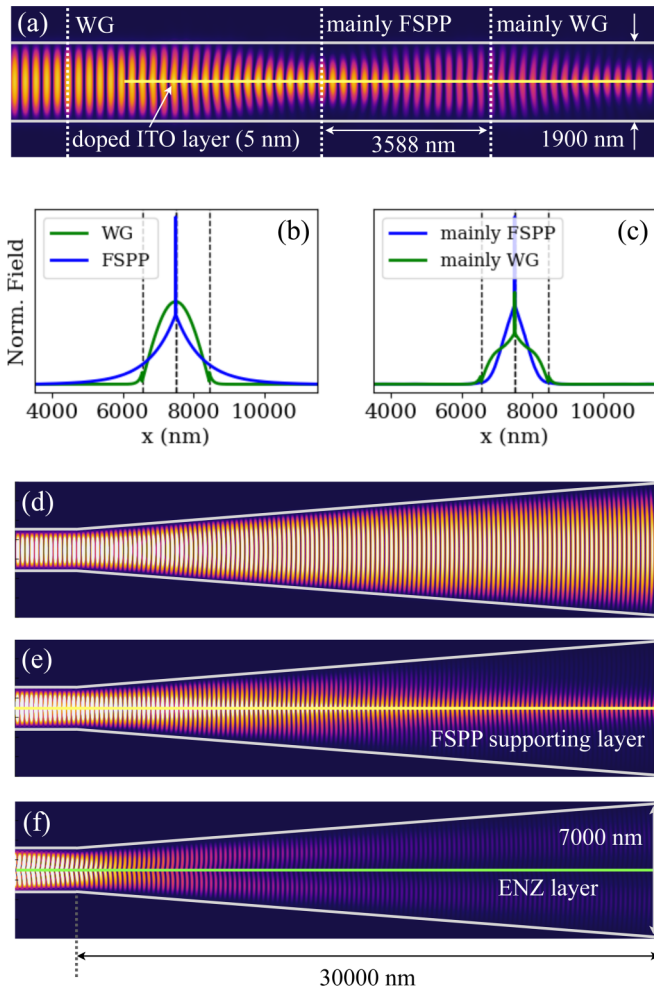


FIG. 3. (a) Hybrid plasmonic waveguide obtained by incorporating a thin FSPP supporting layer (yellow) into an ordinary waveguide. (b) and (c) Pure and hybridized mode field profiles, respectively. (d)–(f) The influence of the FSPP layer (yellow) and ENZ layer (green) on the waveguide mode is demonstrated using the expanding waveguide. Layer thickness is 5 nm, $\lambda = 957$ nm.

interact efficiently. Confining the FSPP inside the waveguide makes it a little bit more lossy and notably more compact. At the same time, the existence of the layer causes a narrow peak to appear in the center of the waveguide mode profile. Corresponding shapes of the hybrid mode during the propagation obtained from the frequency domain simulation are shown in Fig. 3(c). Positions of the cross sections with corresponding profiles are shown in Fig. 3(a) with vertical dashed lines. Despite the obvious attributes of mixing, the original modes are still recognizable. One important conclusion from this picture is that the FSPP can be excited without grating couplers inside ordinary waveguides using the described conversion mechanism. To do so, one should know the conversion length. In the present example it is 3588 nm. In the right place the waveguide should be smoothly removed, leaving the light in the “mainly FSPP” state. Of course, some losses are expected since the conversion between the components of the hybrid is not perfect.

It is important to note that the waveguide mode is held by the walls of the waveguide (shown using gray lines), while the FSPP mode is stuck to the layer. This is a qualitative difference between the propagation of two classical coupled modes in a waveguide and the picture shown in Fig. 3. The second important conclusion from the presented numerical experiment is that the FSPP mode is held by a layer which occupies just 0.3% of the waveguide volume. Just a 5-nm-thick layer in a 2- μm -wide waveguide, with a density of electrons much smaller compared with usual metals, may cause a quite significant effect.

To clearly demonstrate the importance of the embedded layer as well as the difference between the FSPP and ENZ regimes, we perform another numerical experiment presented in Figs. 3(d)–3(f). The waveguide is 3.7 times broader at a distance of 30 μm . In the first example it does not contain any layers, and the light expands together with the waveguide [Fig. 3(d)]. In the second example [Fig. 3(e)] there is an FSPP supporting layer, shown using a yellow line. The result is completely different. The light remains “attached” to the layer in the form of a surface wave. Such a device would realize the FSPP excitation mechanism mentioned above. Note that the propagation length of this particular FSPP is 1.7 times smaller than the length of the device shown in the figure. In the third example [Fig. 3(f)] we exchange the FSPP layer with an ENZ layer. It is quite simple to evaluate the ENZ concentration using Eq. (1). In this particular case, $n_{\text{enz}} \approx 2 \times 10^{21} \text{ cm}^{-3}$ (1.5 times smaller than the FSPP concentration). The result is completely different. The ENZ layer does not support surface modes; it splits and attenuates the mode instead.

As it is approved by numerous models of electro-optical modulators, the ENZ layer is quite an efficient way to attenuate optical modes. Assuming that the layer is tunable (see the next section), it can be integrated directly into a waveguide to manipulate a signal. However, what is more important, a small shift in the density of electrons inside the layer changes the picture completely and allows it to guide surface waves. The dispersion curve [Fig. 2(a)] has a complex structure, and the usage of its different parts may result in very different effects. The meaning of the fine-tuning is to control precisely which part of the curve is in use by choosing the appropriate concentration of electrons. Now, assuming that the accumulation layer can be assembled and disassembled, the existence of the FSPP mode can be switched on and off. Such a mechanism can be extremely useful for future electro-optical devices.

V. REALISTIC CONCENTRATION PROFILES AND SWITCHING

Real-life systems, where tunable FSPP modes are possible, obviously include more physics than we take into account in the analytical model. The simplest system to observe the tuning would be just a thin layer of high-quality dielectric surrounded by a semiconducting material with a well-balanced density of electrons. In this case the external voltage would create an accumulation layer at the boundary with the dielectric. The main difference with the models of Sec. III is that the concentration profile is not a step function, but has a shape that varies smoothly between its maximum and minimum values. The mathematical problem considered in the present section

is to compute properties of FSPP modes supported by tricky concentration profiles and study the possibility to manipulate these plasmons using density profile engineering. The non-rectangular shape, among other things, means that along with the maximal value, the profile also includes other values. If we tune it to have a maximum at the FSPP concentration, we automatically get a point with ENZ concentration (which is slightly below). Moreover, the thickness of the accumulation layer may be effectively thinner than we would prefer it to be. Of course, a semiconducting cladding material has a complex refractive index. The imaginary part can be made small, but it also disturbs the analytics of the previous sections. As a result, the realistic model should be treated numerically.

To compute the concentration, we use the drift-diffusion system of equations. The obtained profiles are used in an optical model based on frequency domain Maxwell equations. The corresponding math is presented in our previous work [23]. Both solvers are realized in COMSOL MULTIPHYSICS software with modules Wave Optics and Semiconductors, correspondingly. The numerical challenge comes from the two length scales in the problem. FSPP modes, which can be quite large, of the order of tenths of micrometers, are supported by a very thin layer with an effective thickness of the order of nanometers. Both parts of the model should be well resolved, and for that reason, strongly inhomogeneous mesh should be used. Another computational difficulty is related to the fact that in the extreme regimes (thin layers, large wavelengths), FSPP effective indices may be very close to the plane waves. To find and identify these modes numerically, one should know exactly where to search. For this reason the analytics of the previous sections is very helpful and sometimes absolutely necessary. As it appears, Eq. (9) well describes the properties of realistic FSPP qualitatively. It also can be used to obtain a reasonable numerical evaluation (see below).

The drift-diffusion equations that we use are quite successful in describing nanoscale semiconducting systems [this approach is used for the modeling of metal-oxide-semiconductor field-effect transistors (MOSFETs) for industrial applications]. Among other things, the theory predicts properties of the accumulation layer quite precisely. At the same time, the electrons in our system are trapped in a thin layer, and a question about possible quantum effects appears. Quantum corrections could be evaluated in alternative approaches, such as, for example, the quantum hydrodynamic model. The influence of Fermi pressure, Bohm potential, exchange-correlation interaction, and spin polarization on the dispersion relation of plasmons is demonstrated using this approach [48,49]. As is indicated in these papers, such corrections play a role in electron gases of high density. In the case of an Au sample analyzed in these works, the density of electrons is $6 \times 10^{22} \text{ cm}^{-3}$. The theory predicts certain corrections in this case, but no qualitative changes in the dispersion curves are observed. In our work we operate with semiconductors with typical densities of about 10^{19} - 10^{21} cm^{-3} . The maximal local concentration that we obtain as a result of manipulation with the charge density distribution using an external potential is approximately an order of magnitude smaller than the typical concentration in gold. For this reason we do not expect any measurable influence of these corrections on our results.

In the previous sections we studied the upper limit for the concentration and FSPP frequencies in ITO, which is close to $\lambda = 843 \text{ nm}$. In this section we choose the wavelength $\lambda = 1550 \text{ nm}$ belonging to the telecom C + L range, which is frequently used in the applications. Practically, this leads to larger FSPP modes and allows us to use slightly smaller concentrations and voltages. More specifically, according to the analytical model, the mean concentration in the accumulation layer should be not less than 10^{21} cm^{-3} .

Models considered here consist of a 10-nm-thick layer of the high-quality insulator HfO_2 with a static permittivity $\bar{\epsilon} = 25$ (or a couple of such layers) surrounded by ITO. The density of charges in the claddings is 10^{19} cm^{-3} . Such a concentration allows ITO to be transparent enough in IR and, at the same time, conductive. For example, a 1900-nm-thick waveguide, similar to the one presented in a previous section, made from such ITO supports classical optical TM modes with propagation length of $\sim 460 \mu\text{m}$ at the wavelength 957 nm. In contrast to the analytical model the medium is dispersive here, and the propagation length at the wavelength 1550 nm is smaller, around $170 \mu\text{m}$. From the point of view of the propagation length, shorter wavelengths are slightly more preferable, but both distances are large enough for experimental verification. The lengths can be increased further by decreasing the doping level in ITO. In this section we consider only purely plasmonic modes, but a hybridization experiment similar to the one discussed in the previous section is, of course, possible.

Typical concentration profiles obtained for the described system are presented in Fig. 4(a) for different voltages. The charge is accumulated at the right boundary of the ITO and dielectric, and the profile decays exponentially into the bulk of the ITO. At the opposite boundary one gets the depletion layer. Since the initial concentration is 10^{19} cm^{-3} and the

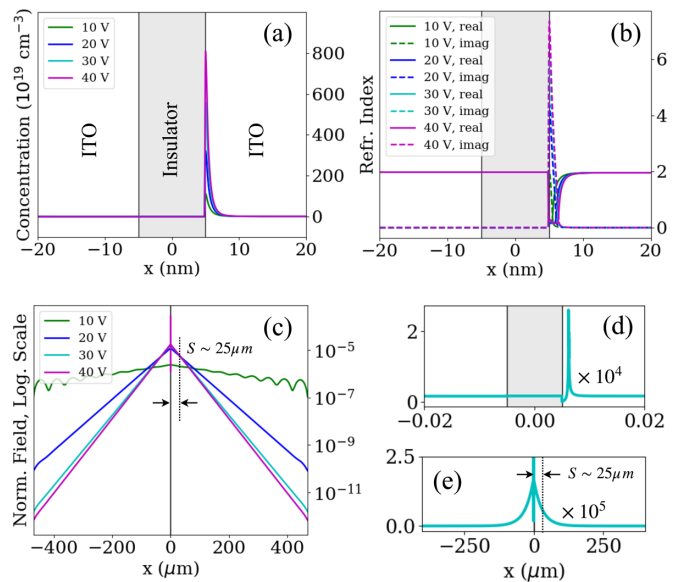


FIG. 4. Tunable FSPP mode in the constructive scheme. (a) Charge concentration profiles for different voltages. (b) Corresponding refractive indices (both real and imaginary parts). (c) Normalized field profiles of FSPP modes plotted in log scale. (d) and (e) Details of the plasmonic field distribution profiles.

depletion profile varies between 0 and 10^{19} , it is not recognizable in Fig. 4(a). The density of charges in the insulating layer is close to zero. The thickness of the accumulation layer is obviously quite small. Moreover, since the profile is not rectangular, it contains a range of values between 10^{19} and approximately 800×10^{19} (the maximum value depends on the voltage), which unavoidably includes the ENZ point along with the FSPP point. This has an influence on the shape and properties of plasmons supported by such a layer.

The refractive index profiles associated with the calculated density profiles via Eq. (1) are shown in Fig. 4(b). Outside the accumulation layer the junction demonstrates almost dielectric properties. Both HfO_2 and ITO have similar values of the dynamic permittivity close to 4. There is also a small jump in the depletion layer. Both jumps are too small to be visible in Fig. 4(b). Doped ITO also possesses a small imaginary part of the permittivity of the order of 10^{-3} . At the position of the accumulation layer this value grows significantly, assuming that the voltage is sufficient to fulfill the FSPP excitation condition.

Plasmonic modes supported by the accumulation layer at different voltages are shown in Fig. 4(c). The electric field norm is plotted as a function of distance from the layer in the log scale. Obviously, no FSPP modes are possible at zero voltage, since the refraction index profile is almost flat in this regime. According to the computations, 10 V are not enough to reach the mean value of concentration necessary to support FSPP. Our numerical solver cannot clearly recognize the corresponding mode and distinguish it from other higher-order modes (green curve). Starting from 20 V, we observe well-recognizable plasmonic modes. The value of the switching voltage can be decreased, if necessary, using more thin insulating layers and high-quality dielectrics with larger static permittivity [50,51]. The shape of the 30-V plasmon field is plotted separately in Fig. 4(e). Along with the classical profile decaying exponentially in both directions from the layer, it has an unusual shape near the accumulation layer that is attributed to the nonrectangular refraction index distribution. The detailed field profile near the accumulation layer is shown in Fig. 4(d).

The size of the obtained modes at the wavelength $\lambda = 1550$ nm is of the order of $25 \mu\text{m}$. Although this is not exactly small, such modes can be used for some applications, for example, to pass optical messages through the body of an appropriately prepared silicon-on-insulator (SOI) wafer, while the surface of the wafer can be used for traditional electronic schemes. Besides, the obtained value characterizes an idealized case with two semi-infinite pieces of ITO, but it does not mean that the obtained plasmons cannot be compressed down to a certain extent using a more complicated geometry. For example, the accumulation layer can be created inside a waveguide, as in Sec. IV, that provides additional compression.

As is clear from the analytical model of the previous sections, the size depends strongly on the thickness of the accumulation layer. A change of thickness of just a few nanometers may cause a significant difference. Unfortunately, variation of the voltage does not change much the thickness of the accumulation layer, but rather its maximum value. To

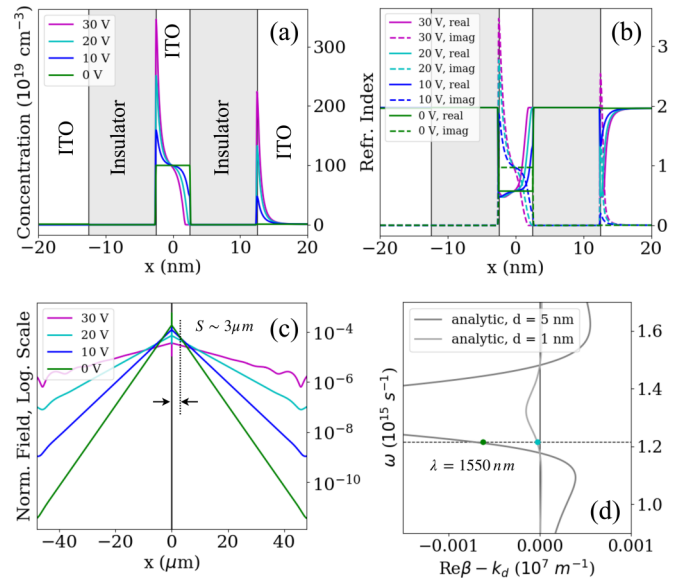


FIG. 5. Tunable FSPP mode in the destructive scheme. (a) Charge concentration profiles for different voltages. (b) Corresponding refractive indices. (c) Normalized field profiles of FSPP modes plotted in log scale. (d) Both constructive and destructive plasmons (cyan and green dots, respectively) placed on the dispersion curve.

increase the thickness, one should think about more tricky geometries. Along with the “constructive approach” implemented above, where the accumulation layer is created by voltage, we may use a “destructive approach,” where one starts with a layer of a necessary width and concentration, provided by the structure of the sandwich and distorts it using the voltage to make the propagation of plasmons impossible. Such a configuration is suggested in Fig. 5(a). Two identical insulating layers are surrounded by ITO. Between the insulators we incorporate a 5-nm-thick layer of highly doped ITO with a concentration of electrons of 10^{21} cm^{-3} . Without the applied voltage, such a system provides a rectangular profile of concentration. The corresponding FSPP mode is shown in Fig. 5(c) (green curve). Its size is just $3 \mu\text{m}$, which is eight times smaller than the corresponding plasmon in Fig. 4(c) (cyan curve). This significant change in size corresponds to the variation of the effective thickness between approximately 1 and 5 nm and agrees well with the analytical model.

The influence of voltage on the plasmonic mode in the “destructive scheme” is shown in Fig. 5. The presented junction is equivalent to the scheme with two capacitors, where two accumulation layers and two depletion layers are formed. In contrast with the “constructive scheme” the depletion layer in the middle is clearly visible [Fig. 5(a)], since the original concentration is high. As is shown, the FSPP vanishes smoothly starting from 20 V, when the distortion of the concentration profile becomes significant enough [Fig. 5(c)].

The numerical model considered here is much more computationally demanding than the analytical description of Sec. III. Nontrivial charge density profiles are taken into account, and ITO claddings are treated as a dispersive medium with a frequency-dependent permittivity. Altogether, it allows

us to obtain much more accurate and detailed results. However, Eq. (9) still can be used to describe the system qualitatively. Figure 5(d) shows the dispersion curves plotted using the analytical formula with a charge concentration of $0.96 \times 10^{21} \text{ cm}^{-3}$ and layer widths of 1 and 5 nm. Two dots (cyan and green) correspond to two plasmons considered here in constructive and destructive schemes, respectively. Therefore a slight variation of the concentration in Eq. (9) allows us to fit the results of the numerical experiment.

Our results demonstrate that both constructive and destructive approaches may provide switching. FSPP modes are supported even by very thin accumulation layers at the standard telecom wavelength $\lambda = 1550 \text{ nm}$. The nontrivial shape of the accumulation layer causes additional fine structure to appear on top of the usual plasmonic field distribution [Figs. 4(d) and 4(e)], but it does not change much their localization and propagation characteristics. Typically, FSPP modes supported by a single accumulation layer are large but highly tunable and can be used for some applications. In general, to obtain smaller tunable modes, it is preferable to use smaller wavelengths and thicker accumulation layers. One of the ways to increase the thickness and significantly decrease the size is demonstrated in this section.

Other methods of charge density profile engineering can be proposed. Some smart manipulation of the band structure may be used to obtain more complicated profiles. Along with ITO, other materials with intermediate density of charges can be considered in the context of switching. Viewing the results of the present section, it is hard to ignore the emerging analogy between field-effect transistors, where the accumulation layer controls a current between a source and a drain, and the electro-optical switching mechanism studied here, where the accumulation layer allows one to guide FSPP.

VI. CONCLUSION

In this paper we discuss the idea of using accumulation layers at ITO-insulator boundaries as highly tunable FSPP carrying waveguides. The simplified analytical formula presented here can be used to describe plasmons in thin layers of highly doped ITO in a dielectric or almost dielectric environment. The formula is also applicable for the approximate description of dynamically assembled accumulation layers inside ITO with low doping level. The analytical approach allows us to evaluate properties of such plasmons, such as the size and propagation length, in various regimes. It is also used to compare the FSPP regime with the ENZ regime frequently used in plasmonic modulators. Quality factors of thin film plasmons in ITO are significantly larger compared with single-interface SPP. This makes them potentially useful for applications.

The detailed numerical analysis based on Maxwell equations and drift-diffusion equations demonstrates the possibility to create and destroy FSPP supporting layers using the applied voltage. The specific shape of concentration profiles, explicitly taken into account in the numerical calculations, results in the appearance of additional features above the usual plasmonic field distribution. In some of the regimes, FSPP modes can be large, but there are always ways to make them smaller by varying the layer thickness and the wavelength.

One of the schemes, allowing us to decrease them to a size eight times smaller, is discussed in the paper. FSPP modes can be compressed further by placing them inside a hybrid waveguide. The main advantage of FSPP modes is their high tunability; thereby they can be used to manipulate optical signals (similar to ENZ modulators). Along with that, the possibility to create and annihilate high-quality plasmonic waveguides dynamically can be used as a basic principle in the new generation of opto-electronics.

APPENDIX: STABILITY OF FSPP MODES WITH RESPECT TO SURFACE IMPERFECTIONS

Surface plasmons are in general quite robust to surface imperfections if their size is large compared with the size of the imperfections. This is one more reason that makes FSPPs

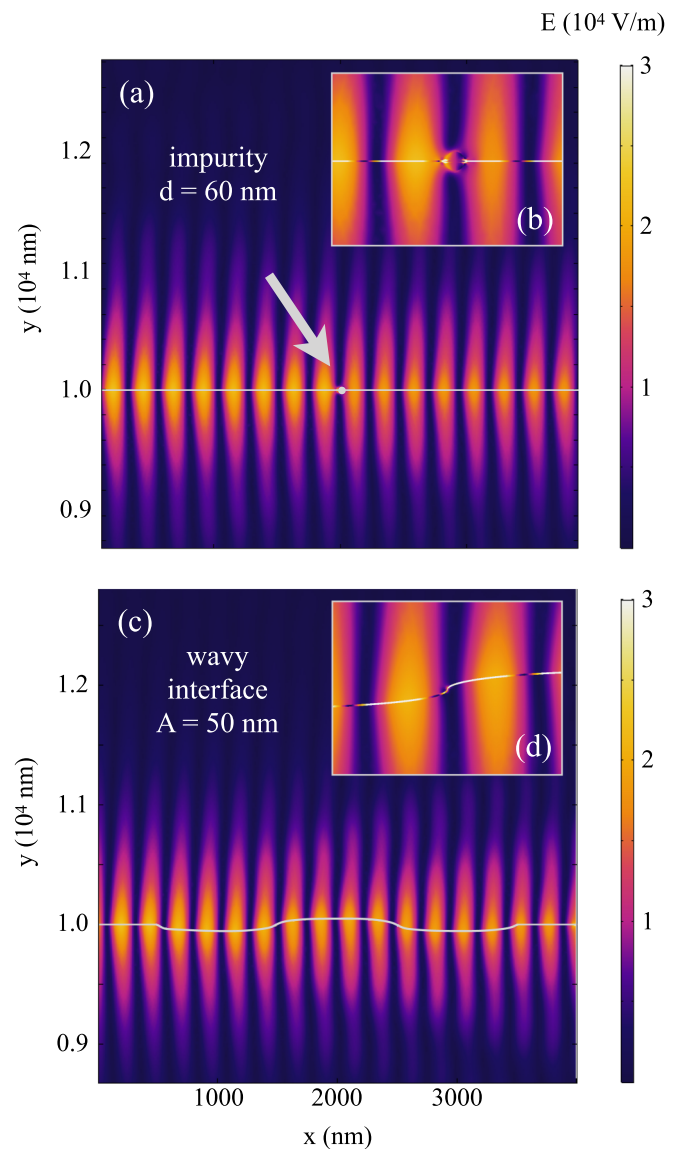


FIG. 6. Influence of surface imperfections on the propagation of FSPP modes. (a) Circular impurity with a diameter $d = 60 \text{ nm}$. (b) Close-up showing the distribution of the field near the impurity. (c) Wavy aberration of the interface with an amplitude $A = 50 \text{ nm}$. (d) Field distribution in the vicinity of the interface.

useful for possible practical applications, since their size is of the order of micrometers (or more) and it is much larger than the typical size of imperfections in modern experiments. The minimalistic structure required to observe FSPP modes is quite simple. One needs to provide an ITO-insulator interface, where the accumulation layer can be formed under the influence of voltage. Practically, the only source of imperfections in this case is a surface roughness. ITO-insulator interfaces can be manufactured with a high accuracy of the order of 10 nm (or even less). This means that the relative size of possible imperfections is practically negligible.

FSPPs are not topologically protected unidirectional modes [52], and some backscattering caused by imperfections

is possible. We present additional computation results to prove that this effect is small for the expected size of defects. The results are summarized in Fig. 6, where the spatial distribution of the electric field norm is shown (color coded). Two types of imperfections are considered: a single circular impurity with a diameter $d = 60$ nm at the interface [Fig. 6(a)] and a wavy boundary with an amplitude $A = 50$ nm [Fig. 6(c)]. The details of the field distribution in the vicinity of the defects are shown in corresponding close-ups [Figs. 6(b) and 6(d), respectively]. In both cases the size of the imperfections is notably larger than the expected experimental inaccuracy of the interface. Our demonstration shows that the influence of such perturbations on FSPP modes is practically negligible.

-
- [1] L. Novotny and B. Hecht, *Principles of Nano-optics* (Cambridge University Press, Cambridge, 2012).
- [2] S. Datta, *Electronic Transport in Mesoscopic Systems* (Cambridge University Press, Cambridge, 1997).
- [3] V. Agranovich and D. Mills, *Surface Polaritons* (North-Holland, Amsterdam, 1982).
- [4] D. Basov, M. Fogler, and F. G. de Abajo, *Science* **354**, aag1992 (2016).
- [5] I. A. Pshenichnyuk, S. S. Kosolobov, and V. P. Drachev, *Appl. Sci.* **9**, 4834 (2019).
- [6] K. Lagoudakis, *The Physics of Exciton-Polariton Condensates* (EPFL Press, Lausanne, 2013).
- [7] L. A. Smirnov, D. A. Smirnova, E. A. Ostrovskaya, and Y. S. Kivshar, *Phys. Rev. B* **89**, 235310 (2014).
- [8] I. Pshenichnyuk, *New J. Phys.* **19**, 105007 (2017).
- [9] I. A. Pshenichnyuk, *Lett. Mater.* **5**, 385 (2015).
- [10] I. A. Pshenichnyuk, *Phys. Lett. A* **382**, 523 (2018).
- [11] T. C. H. Liew, A. V. Kavokin, T. Ostatnický, M. Kaliteevski, I. A. Shelykh, and R. A. Abram, *Phys. Rev. B* **82**, 033302 (2010).
- [12] N. G. Berloff, M. Silva, K. Kalinin, A. Askitopoulos, J. D. Töpfer, P. Cilibizzi, W. Langbein, and P. G. Lagoudakis, *Nat. Mater.* **16**, 1120 (2017).
- [13] W. L. Barnes, A. Dereux, and T. W. Ebbesen, *Nature (London)* **424**, 824 (2003).
- [14] M. I. Stockman, K. Kneipp, S. I. Bozhevolny, S. Saha, A. Dutta, J. Ndukaife, N. Kinsey, H. Reddy, U. Guler, V. M. Shalaev, A. Boltasseva, B. Gholipour, H. N. S. Krishnamoorthy, K. F. MacDonald, C. Soci, N. I. Zheludev, V. Savinov, R. Singh, P. Gross, C. Lienau *et al.*, *J. Opt. (Bristol)* **20**, 043001 (2018).
- [15] D. K. Gramotnev and S. I. Bozhevolnyi, *Nat. Photon.* **4**, 83 (2010).
- [16] E. Ozbay, *Science* **311**, 189 (2006).
- [17] K. Liu, C. R. Ye, S. Khan, and V. J. Sorger, *Laser Photon. Rev.* **9**, 172 (2015).
- [18] A. Melikyan, N. Lindenmann, S. Walheim, P. Leufke, S. Ulrich, J. Ye, P. Vincze, H. Hahn, T. Schimmel, C. Koos, W. Freude, and J. Leuthold, *Opt. Express* **19**, 8855 (2011).
- [19] G. Sinatkas, A. Ptilakis, D. C. Zografopoulos, R. Beccherelli, and E. E. Kriezis, *J. Appl. Phys. (Melville, NY)* **121**, 023109 (2017).
- [20] H. W. Lee, G. Papadakis, S. P. Burgos, K. Chander, A. Kriesch, R. Pala, U. Peschel, and H. A. Atwater, *Nano Lett.* **14**, 6463 (2014).
- [21] V. J. Sorger, N. D. Lanzillotti-Kimura, R.-M. Ma, and X. Zhang, *Nanophotonics* **1**, 17 (2012).
- [22] J. A. Dionne, K. Diest, L. A. Sweatlock, and H. A. Atwater, *Nano Lett.* **9**, 897 (2009).
- [23] I. A. Pshenichnyuk, G. I. Nazarikov, S. S. Kosolobov, A. I. Maimistov, and V. P. Drachev, *Phys. Rev. B* **100**, 195434 (2019).
- [24] Z. Ma, Z. Li, K. Liu, C. Ye, and V. J. Sorger, *Nanophotonics* **4**, 198 (2015).
- [25] M. Noginov, L. Gu, J. Livenere, G. Zhu, A. Pradhan, R. Mundle, M. Bahoura, Y. A. Barnakov, and V. Podolskiy, *Appl. Phys. Lett.* **99**, 021101 (2011).
- [26] G. J. Exarhos and X.-D. Zhou, *Thin Solid Films* **515**, 7025 (2007).
- [27] V. E. Babicheva, A. Boltasseva, and A. V. Lavrinenko, *Nanophotonics* **4**, 165 (2015).
- [28] G. V. Naik, V. M. Shalaev, and A. Boltasseva, *Adv. Mater. (Weinheim)* **25**, 3264 (2013).
- [29] N. Kinsey, C. Devault, A. Boltasseva, and V. M. Shalaev, *Nat. Rev. Mater.* **4**, 742 (2019).
- [30] X. Niu, X. Hu, S. Chu, and Q. Gong, *Adv. Opt. Mater.* **6**, 1701292 (2018).
- [31] L. Ju, B. Geng, J. Horng, C. Girit, M. Martin, Z. Hao, H. A. Bechtel, X. Liang, A. Zettl, Y. R. Shen, and F. Wang, *Nat. Nanotechnol.* **6**, 630 (2011).
- [32] H. Yan, X. Li, B. Chandra, G. Tulevski, Y. Wu, M. Freitag, W. Zhu, P. Avouris, and F. Xia, *Nat. Nanotechnol.* **7**, 330 (2012).
- [33] C. Rhodes, M. Cerruti, A. Efremenko, M. Losego, D. Aspnes, J.-P. Maria, and S. Franzen, *J. Appl. Phys. (Melville, NY)* **103**, 093108 (2008).
- [34] F. Michelotti, L. Dominici, E. Descrovi, N. Danz, and F. Menchini, *Opt. Lett.* **34**, 839 (2009).
- [35] P. Guo, R. D. Schaller, J. B. Ketterson, and R. P. Chang, *Nat. Photon.* **10**, 267 (2016).
- [36] A. Kulkarni and S. Knickerbocker, *J. Vac. Sci. Technol. A* **14**, 1709 (1996).
- [37] M. Alam, I. De Leon, and R. Boyd, *Science* **352**, 795 (2016).
- [38] J. D. Caldwell, L. Lindsay, V. Giannini, I. Vurgaftman, T. L. Reinecke, S. A. Maier, and O. J. Glembocki, *Nanophotonics* **4**, 44 (2015).
- [39] M. Bender, W. Seelig, C. Daube, H. Frankenberger, B. Ocker, and J. Stollenwerk, *Thin Solid Films* **326**, 72 (1998).

- [40] H. Kim, a. C. Gilmore, A. Pique, J. Horwitz, H. Mattoussi, H. Murata, Z. Kafafi, and D. Chrisey, *J. Appl. Phys. (Melville, NY)* **86**, 6451 (1999).
- [41] J. George and C. Menon, *Surf. Coat. Technol.* **132**, 45 (2000).
- [42] F. Kurdesau, G. Khripunov, A. Da Cunha, M. Kaelin, and A. Tiwari, *J. Non-Cryst. Solids* **352**, 1466 (2006).
- [43] S. A. Maier, *Plasmonics: Fundamentals and Applications* (Springer, New York, 2007).
- [44] J. J. Burke, G. I. Stegeman, and T. Tamir, *Phys. Rev. B* **33**, 5186 (1986).
- [45] P. N. Melentiev, A. Kalmykov, A. Kuzin, D. Negrov, V. Klimov, and V. I. Balykin, *ACS Photon.* **6**, 1425 (2019).
- [46] M. Z. Alam, J. S. Aitchison, and M. Mojahedi, *Laser Photon. Rev.* **8**, 394 (2014).
- [47] M. Alam, J. S. Aitchison, and M. Mojahedi, *IEEE J. Sel. Top. Quantum Electron.* **19**, 4602008 (2013).
- [48] M. Shahmansouri and M. Mahmodi Moghadam, *Phys. Plasmas* **24**, 102107 (2017).
- [49] S. Majedi, S. Khorashadizadeh, and A. Niknam, *Eur. Phys. J. Plus* **133**, 77 (2018).
- [50] G. D. Wilk, R. M. Wallace, and J. Anthony, *J. Appl. Phys. (Melville, NY)* **89**, 5243 (2001).
- [51] J. Robertson, *Eur. Phys. J.: Appl. Phys.* **28**, 265 (2004).
- [52] S. A. H. Gangaraj and F. Monticone, *J. Phys.: Condens. Matter* **30**, 104002 (2018).